

Study of the Processes $e^+e^- \rightarrow \eta\gamma$, $\pi^0\gamma \rightarrow 3\gamma$ in the c.m. Energy Range 600–1380 MeV at CMD-2

R.R. Akhmetshin ^a, V.M. Aulchenko ^{a,c}, V.Sh. Banzarov ^a,
 A. Baratt ^d, L.M. Barkov ^{a,c}, N.S. Bashtovoy ^a, A.E. Bondar ^{a,c},
 D.V. Bondarev ^a, A.V. Bragin ^a, S.I. Eidelman ^{a,c},
 D.A. Epifanov ^a, G.V. Fedotovitch ^{a,c}, N.I. Gabyshev ^a,
 D.A. Gorbachev ^a, A.A. Grebeniuk ^a, D.N. Grigoriev ^a,
 F.V. Ignatov ^a, S.V. Karpov ^a, V.F. Kazanin ^{a,c}, B.I. Khazin ^{a,c},
 I.A. Koop ^{a,c}, P.P. Krovovny ^{a,c}, A.S. Kuzmin ^{a,c},
 Yu.E. Lischenko ^a, I.B. Logashenko ^a, P.A. Lukin ^a,
 K.Yu. Mikhailov ^a, A.I. Milstein ^{a,c}, I.N. Nesterenko ^{a,c},
 V.S. Okhapkin ^a, A.V. Otboev ^{a,c}, A.S. Popov ^a, S.I. Redin ^a,
 B.L. Roberts ^b, N.I. Root ^a, A.A. Ruban ^a, N.M. Ryskulov ^a,
 A.G. Shamov ^a, Yu.M. Shatunov ^a, B.A. Shwartz ^{a,c},
 A.L. Sibidanov ^{a,c}, V.A. Sidorov ^a, A.N. Skrinsky ^a,
 I.G. Snopkov ^a, E.P. Solodov ^{a,c}, J.A. Thompson ^{d 1},
 A.A. Valishev ^a, Yu.V. Yudin ^a, A.S. Zaitsev ^{a,c}, S.G. Zverev ^a

^a*Budker Institute of Nuclear Physics, Novosibirsk, 630090, Russia*

^b*Boston University, Boston, MA 02215, USA*

^c*Novosibirsk State University, Novosibirsk, 630090, Russia*

^d*University of Pittsburgh, Pittsburgh, PA 15260, USA*

^e*Yale University, New Haven, CT 06511, USA*

¹ deceased

Abstract

The processes $e^+e^- \rightarrow \eta\gamma$, $\pi^0\gamma \rightarrow 3\gamma$ have been studied in the c.m. energy range 600–1380 MeV with the CMD-2 detector. The following branching ratios have been determined:

$$\begin{aligned}\mathcal{B}(\rho^0 \rightarrow \eta\gamma) &= (3.21 \pm 1.39 \pm 0.20) \cdot 10^{-4}, \\ \mathcal{B}(\omega \rightarrow \eta\gamma) &= (4.44_{-1.83}^{+2.59} \pm 0.28) \cdot 10^{-4}, \\ \mathcal{B}(\phi \rightarrow \eta\gamma) &= (1.373 \pm 0.014 \pm 0.085) \cdot 10^{-2}, \\ \mathcal{B}(\rho^0 \rightarrow \pi^0\gamma) &= (6.21_{-1.18}^{+1.28} \pm 0.39) \cdot 10^{-4}, \\ \mathcal{B}(\omega \rightarrow \pi^0\gamma) &= (9.06 \pm 0.20 \pm 0.57) \cdot 10^{-2}, \\ \mathcal{B}(\phi \rightarrow \pi^0\gamma) &= (1.258 \pm 0.037 \pm 0.077) \cdot 10^{-3}.\end{aligned}$$

1 Introduction

The magnetic dipole transitions of the light vector mesons (ρ , ω and ϕ) to the $\pi^0\gamma$ and $\eta\gamma$ final states have traditionally provided a convenient laboratory for various tests of theoretical concepts, particularly the nonrelativistic quark model and Vector Dominance Model (VDM) [1,2]. There are ongoing discussions about mechanisms of SU(3) breaking, possible admixture of glue in mesons and the role of anomalies in radiative decays [3,4,5,6,7,8]. Precise measurements of the cross sections of e^+e^- annihilation into the $\pi^0\gamma$ and $\eta\gamma$ final states in the broad c.m.energy range are necessary for the problem of the muon anomaly [9]. Radiative decays to $\pi^0\gamma$ and $\eta\gamma$ can also provide important information on the properties of the ρ , ω and ϕ excitations as well as on the existence of light hybrids between 1000 and 2000 MeV [10,11].

Despite previous experimental efforts (cf. the detailed bibliography in [12]), of these decays only $\omega \rightarrow \pi^0\gamma$ and $\phi \rightarrow \eta\gamma$ are rather well studied. A three-photon final state is convenient for the investigation of the $\pi^0\gamma$ and $\eta\gamma$ final states since both π^0 and η readily decay into two photons. Measurements of the branching ratios for corresponding decays of the ρ , ω and ϕ using the two-photon decay mode have been performed at ND [13,14] and SND [15,16], however, none of them covered the whole off-resonance energy range.

In this work we report on the measurement of the cross section of the processes $e^+e^- \rightarrow \pi^0\gamma$ and $e^+e^- \rightarrow \eta\gamma$ in the three-photon final state in the c.m.energy range 600–1380 MeV using the data from the CMD-2 detector at the VEPP-

2M e^+e^- collider.

2 Experiment

The general purpose detector CMD-2 has been described in detail elsewhere [17]. Its tracking system consists of a cylindrical drift chamber (DC) and double-layer multiwire proportional Z-chamber, both also used for the trigger, and both inside a thin ($0.38 X_0$) superconducting solenoid with a field of 1 T. The barrel CsI calorimeter (BC) with a thickness of $8.1 X_0$ placed outside the solenoid has energy resolution for photons of about 9% in the energy range from 100 to 700 MeV. The angular resolution is of the order of 0.02 radians. The end-cap BGO calorimeter with a thickness of $13.4 X_0$ placed inside the solenoid has energy and angular resolution varying from 9% to 4% and from 0.03 to 0.02 radians, respectively, for the photon energy in the range 100 to 700 MeV. The barrel and end-cap calorimeter systems cover a solid angle of $0.92 \times 4\pi$ radians.

This analysis is based on a data sample corresponding to integrated luminosity of 21 pb^{-1} collected in 1997–1998 in the energy range 600–1380 MeV. The step of the c.m. energy scan varied from 0.5 MeV near the ω and ϕ peaks to 10 MeV far from the resonances. The beam energy spread is about 4×10^{-4} of the total energy. The luminosity is measured using events of Bhabha scattering at large angles [18].

A GEANT3 based Monte Carlo simulation (MC) package is used to model the detector response and determine the efficiency [19]. Because of the beam induced background additional (“fake”) clusters can appear in the calorimeter. To take this effect into account in MC we determine a corresponding probability as well as photon energy and angular spectra directly from the data using the process $e^+e^- \rightarrow \pi^+\pi^-\pi^0$, and then include generation of such photons in the detector response during simulation.

3 Data analysis

At the initial stage, events are selected which have no tracks in the DC, three or four photons in the CsI calorimeter, the total energy deposition $0.8 < E_{\text{tot}}/E_{\text{cm}} < 1.1$, the total momentum $P_{\text{tot}}/E_{\text{cm}} < 0.15$ and the minimum photon energy of 50 MeV. Figure 1 (left) shows the E_{tot} distribution for the data and signal MC near the ϕ resonance. One can see good agreement between

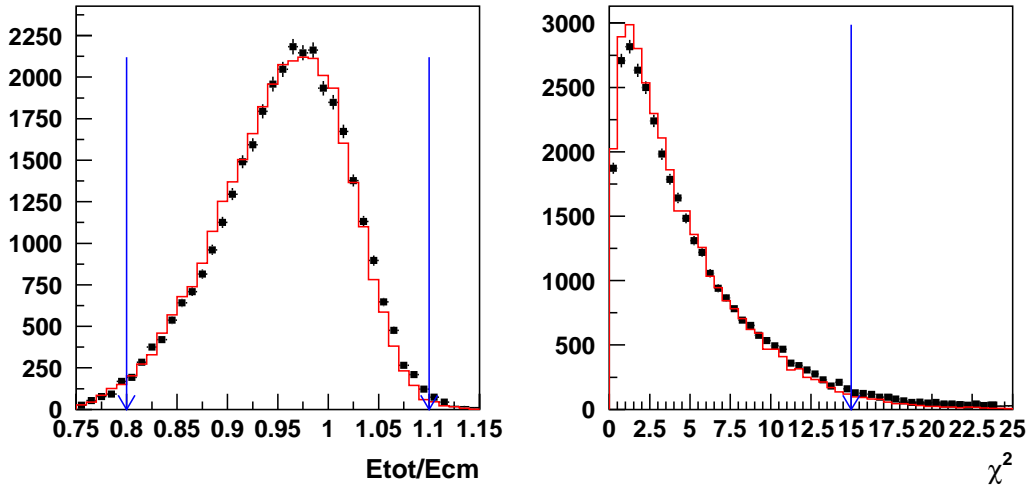


Fig. 1. The $E_{\text{tot}}/E_{\text{cm}}$ (left) and χ^2 (right) distributions. The points with error bars represent experimental events, the histograms show the MC simulation. The arrows indicate the cuts imposed.

the data and signal MC. About 52×10^3 events were selected in the whole energy range after these requirements.

Then a kinematic fit requiring energy-momentum conservation and good reconstruction quality ($\chi^2 < 15$, see Fig. 1 (right)) was performed. The reconstruction procedure assumes three photons, i.e., for events with four photons a combination of three photons with the minimum χ^2 is chosen. After this stage about 48×10^3 events remain.

The dominant background comes from the QED three-photon annihilation: $e^+e^- \rightarrow 3\gamma$. These events can not be completely rejected by selection criteria. The $\eta\gamma$, $\pi^0\gamma$ and background events can be separated using decay dynamics. Figure 2 shows the Dalitz plot for the $\phi \rightarrow 3\gamma$ final state. Here the photons are sorted by their energy so that the first photon has a maximum energy: $E_1 > E_2 > E_3$.

The Dalitz plot is divided into three regions: $D_{\eta\gamma}$ ($340 \text{ MeV} < E_2 < 385 \text{ MeV}$ or $E_1 < 385 \text{ MeV}$), $D_{\pi^0\gamma}$ ($491 \text{ MeV} < E_1 < 511 \text{ MeV}$) and D_{bg} (all the remaining events). For each of the three final states ($\eta\gamma$, $\pi^0\gamma$ and QED) we determine from the MC simulation the probabilities to enter each region. Then from the population of various regions of the Dalitz plot in the data the total number of events due to each process is calculated. However, this method can provide bias in the signal yield determination because of the imperfect MC simulation.

Therefore, we obtain the number of $\eta\gamma$ and $\pi^0\gamma$ events by fitting the two-photon invariant mass distribution. The invariant mass of the two softer photons (M_{23}) is used for π^0 reconstruction. For the η signal three combinations

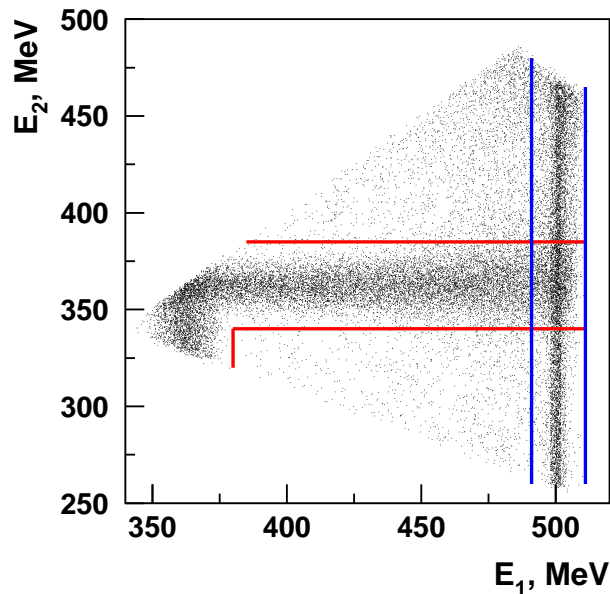


Fig. 2. The Dalitz plot for the 3γ final state at the ϕ meson energy. The points represent experimental events, the lines indicate boundaries used in the selection criteria, see the text for more detail.

are used:

- (1) In case of $E_1 < m_\eta^2/\sqrt{s}$, two hard photons are used (M_{12}).
- (2) Otherwise, if $E_3 < m_\eta^2/\sqrt{s}$, we use the first and third photons (M_{13}).
- (3) In other cases two soft photons (M_{23}) are used.

In most of the cases the shape of the signal distributions is taken from the data, whereas for the background it is taken from the data and MC. Figure 3 shows the two-photon invariant mass distributions for the data and signal MC near the peak of the ϕ meson. The difference in the number of selected events in these two methods (about 3%) was considered as a systematic uncertainty because of the separation procedure.

Other possible sources of background are the processes $e^+e^- \rightarrow \eta\gamma \rightarrow 3\pi^0\gamma$, $e^+e^- \rightarrow K_S K_L$, $e^+e^- \rightarrow \gamma\gamma$ and $e^+e^- \rightarrow \omega\pi^0 \rightarrow \pi^0\pi^0\gamma$. The expected number of events from these processes was calculated from the detection efficiencies determined by the MC simulation and their cross sections independently measured at CMD-2 [20,21,22,23,24]. The fraction of background events is negligible below the ϕ meson, about 2% only in the ϕ meson energy range and dominant in the high energy range. The separation procedure gives 17400 $\eta\gamma$ events, 18680 $\pi^0\gamma$ events and about 12000 QED events.

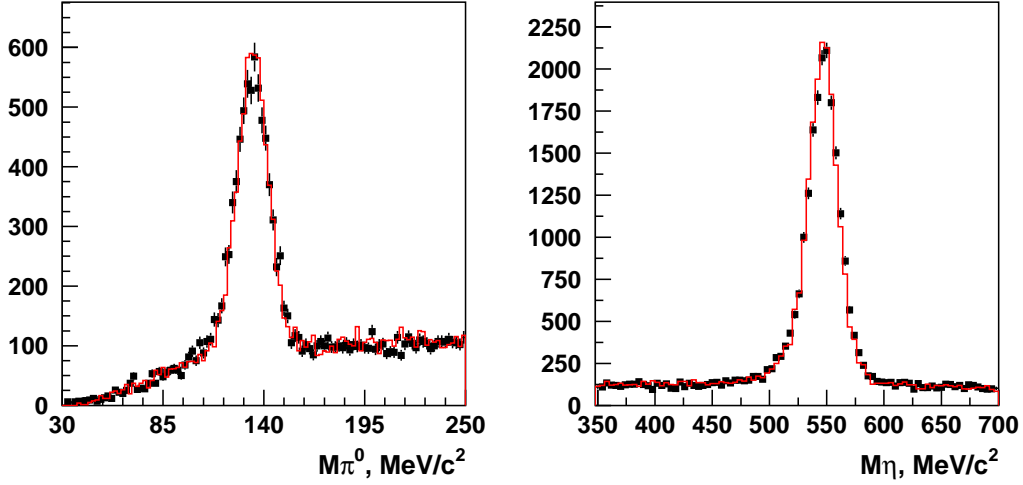


Fig. 3. The two-photon invariant mass distributions in the π^0 (left) and η (right) mass range. The points with error bars represent experimental events, histograms show the MC simulation.

3.1 Approximation of the cross sections

At each energy point the cross section of the process σ is calculated using the following formula:

$$\sigma_i = \frac{N_i}{L_i \varepsilon_i (1 + \delta_i)}, \quad (1)$$

where N_i is the number of selected events, L_i is the integrated luminosity, ε_i is the detection efficiency and $(1 + \delta_i)$ is the radiative correction at the i -th energy point.

The detection efficiency was calculated from the Monte Carlo simulation taking into account corrections obtained from the data and the neutral trigger efficiency. Neutral trigger (NT) is part of the CMD-2 trigger system responsible for events with a final state of photons only, without any charged tracks. The NT efficiency was estimated using events of the process $e^+e^- \rightarrow e^+e^-\gamma$ at each energy point. Its value varied from about 80% to 90%.

The radiative corrections are calculated according to [25]. The dependence of the detection efficiency on the energy of the emitted photon is determined from simulation.

The obtained cross sections of the processes $e^+e^- \rightarrow \eta\gamma, \pi^0\gamma$ are shown in Figs. 4, 5. The detailed information on this analysis is listed in Tables 1-4. The cross section shown there is a so called “dressed” one, which is used in the approximation of the energy dependence with resonances. For applications

Table 1

The c.m. energy, integrated luminosity, number of selected events, detection efficiency, radiative correction, and Born cross section σ of the process $e^+e^- \rightarrow \eta\gamma$.

\sqrt{s} , MeV	L , nb $^{-1}$	N_{exp}	ε , %	$1 + \delta$	σ , nb
599.86	35.2	0.1 ± 2.3	2.3	-0.157	< 4.71
629.86	44.6	0.7 ± 2.8	7.2	-0.142	< 1.68
659.86	39.8	3.0 ± 2.9	11.6	-0.134	0.75 ± 0.63
719.86	56.9	0.0 ± 2.5	15.0	-0.126	< 0.48
749.86	42.9	0.1 ± 1.9	16.0	-0.117	< 0.44
759.86	33.7	3.4 ± 2.7	15.7	-0.115	0.73 ± 0.51
763.86	39.7	5.6 ± 3.9	16.0	-0.116	1.00 ± 0.61
769.86	34.3	0.2 ± 2.1	17.0	-0.126	< 0.63
773.86	70.1	1.0 ± 2.8	15.8	-0.147	0.11 ± 0.26
777.86	83.6	2.4 ± 3.5	15.8	-0.186	0.22 ± 0.27
779.86	56.6	10.0 ± 3.9	14.7	-0.204	1.50 ± 0.46
780.86	58.5	2.3 ± 5.9	8.8	-0.207	0.57 ± 1.14
781.86	366.8	41.2 ± 9.3	14.7	-0.203	0.94 ± 0.18
782.86	77.6	9.8 ± 4.4	15.3	-0.191	1.03 ± 0.37
783.86	71.7	2.1 ± 3.3	15.7	-0.172	0.22 ± 0.29
785.86	67.0	8.2 ± 3.9	16.0	-0.123	0.87 ± 0.36
789.86	28.4	1.5 ± 2.1	15.2	-0.046	0.36 ± 0.48
793.86	46.2	1.7 ± 2.2	15.9	-0.010	0.23 ± 0.31
799.86	56.5	0.9 ± 2.0	15.5	0.005	0.10 ± 0.23
809.86	59.9	3.9 ± 2.7	15.9	0.006	0.41 ± 0.29
819.86	109.4	8.0 ± 4.1	15.8	0.004	0.47 ± 0.24
839.86	130.4	8.6 ± 4.5	15.4	-0.006	0.43 ± 0.23
879.86	167.9	2.1 ± 3.9	15.2	-0.037	0.08 ± 0.15
919.86	285.4	5.7 ± 5.4	15.0	-0.063	0.14 ± 0.13
939.86	136.7	1.1 ± 3.8	15.5	-0.077	0.06 ± 0.18
949.86	226.1	12.5 ± 5.5	16.2	-0.085	0.38 ± 0.15
957.86	250.1	6.2 ± 4.7	16.5	-0.093	0.17 ± 0.12
969.86	249.7	4.7 ± 5.1	17.2	-0.108	0.12 ± 0.12
983.93	307.7	5.2 ± 7.0	20.4	-0.132	0.07 ± 0.13

Table 2

The c.m. energy, integrated luminosity, number of selected events, detection efficiency, radiative correction, and Born cross section σ of the process $e^+e^- \rightarrow \eta\gamma$.

\sqrt{s} , MeV	L , nb $^{-1}$	N_{exp}	ε , %	$1 + \delta$	σ , nb
1003.91	357.7	44.0 ± 10.2	20.3	-0.192	0.67 ± 0.15
1010.53	477.3	109.6 ± 14.9	19.9	-0.227	1.48 ± 0.16
1015.77	391.7	401.3 ± 23.0	20.0	-0.268	6.80 ± 0.30
1016.77	660.1	968.1 ± 34.8	19.6	-0.277	10.00 ± 0.27
1016.91	306.1	497.6 ± 24.9	20.0	-0.277	10.90 ± 0.49
1017.61	673.7	1362.1 ± 40.8	20.1	-0.282	13.77 ± 0.32
1017.77	563.1	1198.8 ± 38.2	19.9	-0.282	14.80 ± 0.44
1018.58	410.1	1230.8 ± 38.4	20.1	-0.278	21.31 ± 0.58
1018.83	977.5	2855.9 ± 57.8	19.9	-0.274	21.13 ± 0.30
1019.50	633.1	1941.9 ± 47.5	20.1	-0.254	21.50 ± 0.43
1019.84	810.8	2584.6 ± 54.6	20.2	-0.238	21.54 ± 0.73
1020.62	876.3	2231.7 ± 51.3	20.0	-0.187	15.52 ± 0.30
1021.54	440.6	800.5 ± 30.9	20.0	-0.112	9.82 ± 0.36
1022.79	551.0	621.5 ± 28.0	20.1	0.007	5.38 ± 0.26
1027.67	562.2	198.9 ± 17.3	20.2	0.591	1.08 ± 0.15
1033.67	510.8	100.0 ± 14.0	19.9	1.557	0.38 ± 0.14
1039.59	447.5	66.5 ± 11.9	20.1	2.911	0.18 ± 0.13
1049.80	312.5	23.4 ± 8.2	19.6	6.778	0.05 ± 0.13
1059.49	220.6	9.8 ± 5.9	19.3	13.272	< 0.30
1079.00	437.0	4.6 ± 6.8	22.7	39.899	< 0.11
1163.40	918.2	0.0 ± 10.3	21.8	0.035	< 0.08
1310.00	4249.0	-0.4 ± 21.6	20.9	-0.074	< 0.05

to various dispersion integrals like that for the leading order hadronic contribution to the muon anomalous magnetic moment, the “bare” cross section should be used [26].

The maximum likelihood method is applied to fit the energy dependence of the experimental cross sections obtained from the relation (1).

The Born cross section of these processes can be written as:

Table 3

The c.m. energy, integrated luminosity, number of selected events, detection efficiency, radiative correction, and Born cross section σ of the process $e^+e^- \rightarrow \pi^0\gamma$.

\sqrt{s} , MeV	L , nb $^{-1}$	N_{exp}	ε , %	$1 + \delta$	σ , nb
599.86	35.2	4.8 ± 3.6	12.0	-0.089	1.23 ± 0.86
629.86	44.6	9.2 ± 4.2	12.8	-0.093	1.78 ± 0.74
659.86	39.8	8.6 ± 4.4	12.5	-0.099	1.92 ± 0.89
719.86	56.9	14.1 ± 5.2	14.0	-0.112	2.00 ± 0.65
749.86	42.9	27.1 ± 5.9	14.3	-0.131	5.08 ± 0.97
759.86	33.7	35.0 ± 6.8	14.7	-0.150	8.31 ± 1.40
763.86	39.7	62.8 ± 8.6	14.5	-0.162	12.97 ± 1.52
769.86	34.3	76.7 ± 9.2	15.5	-0.185	17.64 ± 1.77
773.86	70.1	281.1 ± 17.3	14.6	-0.204	34.33 ± 1.82
777.86	83.6	721.5 ± 27.5	14.4	-0.224	76.65 ± 2.64
779.86	56.6	757.7 ± 27.8	13.8	-0.229	125.81 ± 4.92
780.86	58.5	717.7 ± 27.0	8.6	-0.228	184.98 ± 10.99
781.86	366.8	6619.7 ± 82.0	13.6	-0.221	172.26 ± 2.47
782.86	77.6	1664.6 ± 41.1	14.9	-0.206	183.37 ± 4.80
783.86	71.7	1403.6 ± 37.7	14.9	-0.183	162.00 ± 4.72
785.86	67.0	978.8 ± 31.6	13.9	-0.116	118.44 ± 4.16
789.86	28.4	187.8 ± 13.9	14.6	0.050	42.80 ± 3.80
793.86	46.2	166.2 ± 13.3	14.8	0.217	19.93 ± 2.06
799.86	56.5	134.8 ± 12.2	14.8	0.441	11.18 ± 1.52
809.86	59.9	83.7 ± 9.9	15.5	0.724	5.22 ± 1.09
819.86	109.4	87.9 ± 10.4	15.4	0.906	2.74 ± 0.62
839.86	130.4	61.7 ± 9.2	15.8	0.901	1.58 ± 0.45
879.86	167.9	17.2 ± 6.0	17.2	0.342	0.44 ± 0.21
919.86	285.4	20.8 ± 6.6	17.4	0.021	0.41 ± 0.13
939.86	136.7	18.0 ± 5.5	17.9	0.001	0.74 ± 0.22
949.86	226.1	20.1 ± 6.2	18.0	-0.008	0.50 ± 0.15
957.86	250.1	15.7 ± 5.8	18.4	-0.015	0.35 ± 0.13
969.86	249.7	11.8 ± 5.4	18.6	-0.029	0.26 ± 0.12
983.93	307.7	9.4 ± 6.3	19.9	-0.053	0.16 ± 0.11

Table 4

The c.m. energy, integrated luminosity, number of selected events, detection efficiency, radiative correction, and Born cross section σ of the process $e^+e^- \rightarrow \pi^0\gamma$.

\sqrt{s} , MeV	L , nb $^{-1}$	N_{exp}	ε , %	$1 + \delta$	σ , nb
1003.91	357.7	29.5 ± 8.2	20.5	-0.127	0.44 ± 0.12
1010.53	477.3	50.3 ± 10.1	20.7	-0.179	0.61 ± 0.10
1015.77	391.7	120.9 ± 13.3	20.5	-0.243	1.95 ± 0.17
1016.77	660.1	306.1 ± 20.7	20.4	-0.256	2.95 ± 0.16
1016.91	306.1	175.4 ± 15.3	21.0	-0.257	3.59 ± 0.30
1017.61	673.7	401.4 ± 23.3	20.3	-0.263	3.97 ± 0.18
1017.77	563.1	363.4 ± 22.0	20.5	-0.264	4.29 ± 0.24
1018.58	410.1	347.8 ± 21.5	20.7	-0.260	5.72 ± 0.32
1018.83	977.5	764.3 ± 32.1	20.2	-0.255	5.46 ± 0.17
1019.50	633.1	466.7 ± 25.2	20.7	-0.228	4.77 ± 0.24
1019.84	810.8	591.8 ± 28.5	20.8	-0.208	4.54 ± 0.52
1020.62	876.3	454.3 ± 26.0	20.7	-0.139	2.85 ± 0.15
1021.54	440.6	143.4 ± 15.2	20.6	-0.024	1.52 ± 0.17
1022.79	551.0	114.6 ± 14.0	20.4	0.199	0.78 ± 0.13
1027.67	562.2	35.1 ± 9.2	20.6	2.660	0.08 ± 0.08
1033.67	510.8	13.8 ± 7.5	20.7	43.316	< 0.11
1039.59	447.5	10.4 ± 6.6	20.7	72.963	< 0.11
1049.80	312.5	1.8 ± 5.1	20.4	6.939	< 0.13
1059.49	220.6	2.0 ± 5.3	20.4	3.314	< 0.20
1079.00	437.0	-0.6 ± 5.5	27.4	1.634	< 0.08
1163.40	918.2	19.8 ± 9.7	28.1	-0.047	0.08 ± 0.04
1310.00	4249.0	48.1 ± 16.2	26.9	-0.143	0.05 ± 0.02

$$\sigma_{\text{P}\gamma}(s) = \frac{F_{\text{P}\gamma}(s)}{s^{3/2}} \cdot \left| \sum_{\text{V}} A_{\text{V}} \right|^2, \quad (2)$$

$$A_{\text{V}} = \sqrt{\sigma_{\text{V}}^{(0)} \frac{m_{\text{V}}^3}{F(m_{\text{V}}^2)}} \cdot \frac{m_{\text{V}}\Gamma_{\text{V}}e^{i\varphi_{\text{V}}}}{m_{\text{V}}^2 - s - i\sqrt{s}\Gamma_{\text{V}}(s)},$$

where m_{V} is the mass of the resonance, $\Gamma_{\text{V}}(s)$ and $\Gamma_{\text{V}} = \Gamma_{\text{V}}(m_{\text{V}}^2)$ are its width at the squared c.m. energy s and at the resonance peak ($s = m_{\text{V}}^2$), respectively, δ_{V} is its relative phase, $F(s)$ is a factor taking into account the energy dependence of the phase space of the final state, $F_{\text{P}\gamma}(s) = p_{\gamma}^3 = (\sqrt{s}(1 -$

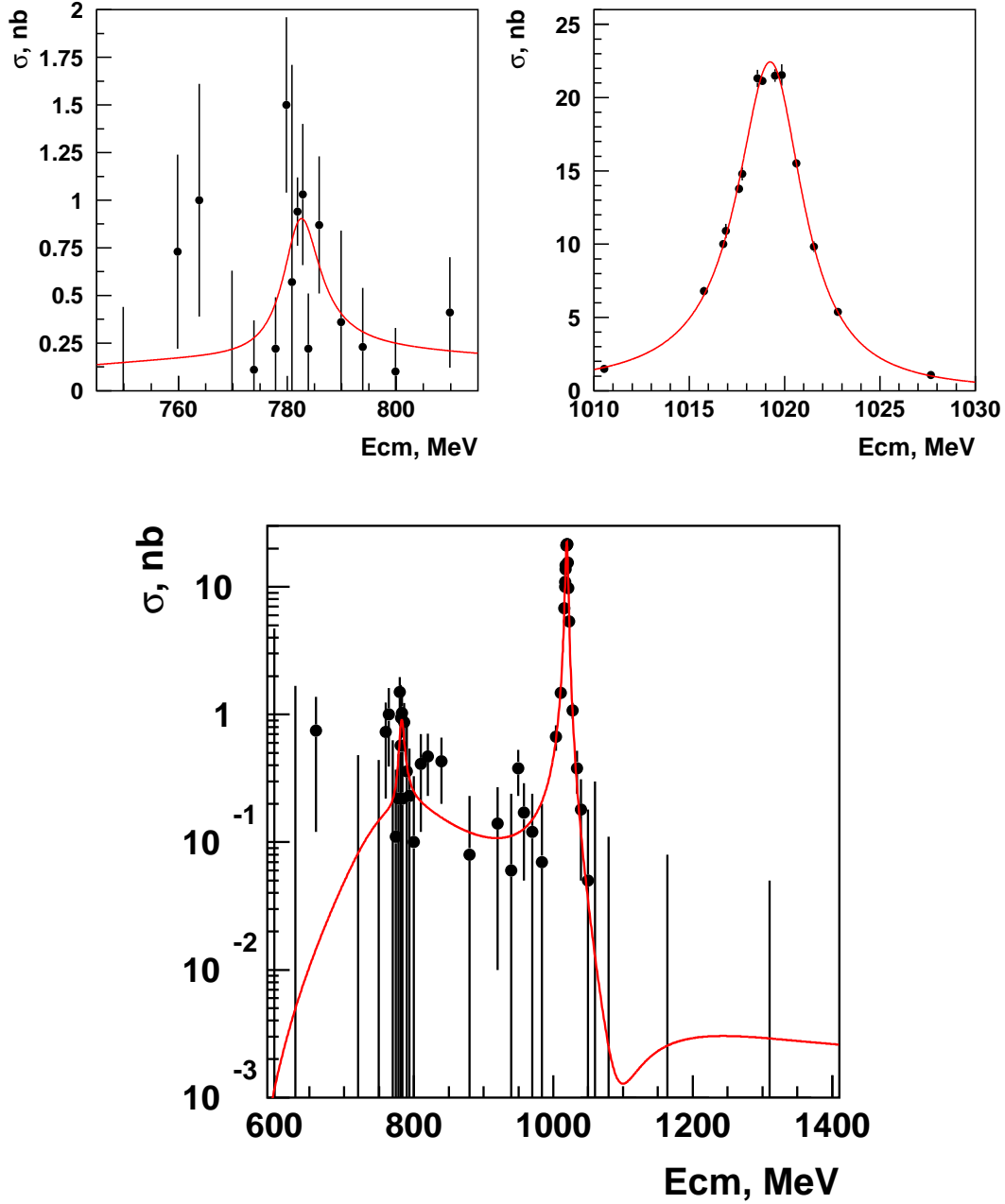


Fig. 4. The cross section of the process $e^+e^- \rightarrow \eta\gamma$. The points with error bars represent the experimental data, the curve corresponds to the result of the fit.

$m_V^2/2s)^3$, $\sigma_V^{(0)}$ is the cross section at the resonance peak:

$$\sigma_V^{(0)} = \sigma_{e^+e^- \rightarrow V \rightarrow \eta\gamma}(m_V^2) = \frac{12\pi B_{V \rightarrow e^+e^-} B_{V \rightarrow \eta\gamma}}{m_V^2}, \quad (3)$$

where $B_{V \rightarrow e^+e^-}$ and $B_{V \rightarrow \eta\gamma}$ are the corresponding branching ratios. In Eq. (2) we sum over all vector mesons relevant at this energy, $V = \rho, \omega, \phi, \rho', \omega'$.

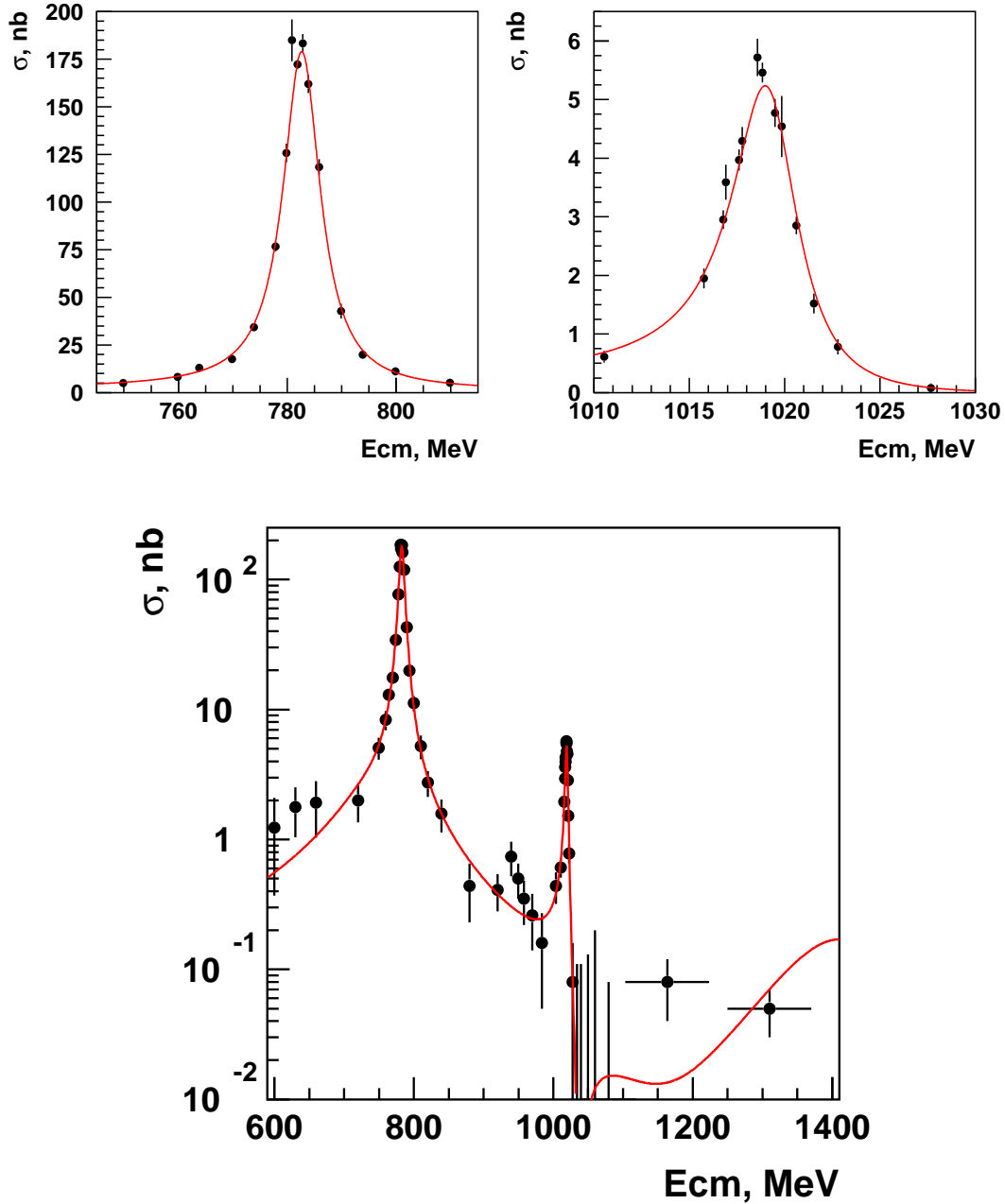


Fig. 5. The cross section of the process $e^+e^- \rightarrow \pi^0\gamma$. The points with error bars represent the experimental data, the curve corresponds to the result of the fit.

The Gounaris-Sakurai model has been used for the description of the ρ meson [27]. To describe the energy dependence of the ω and ϕ meson widths, their main decay modes $\pi^+\pi^-\pi^0$, $\pi^0\gamma$ as well as $K_L^0 K_S^0$, K^+K^- , $\pi^+\pi^-\pi^0$ and $\eta\gamma$, respectively, were taken into account using the same parameterization as in [28]. For the $\rho'(1450)$ the energy dependence of the width assumed 60% and 40% branching ratios for its decays into $a_1(1260)\pi$ and $\omega\pi$, respectively [29]. Its mass and width were taken to be 1465 MeV and 400 MeV,

Table 5

Results of the fits for the processes $e^+e^- \rightarrow \eta\gamma$ and $e^+e^- \rightarrow \pi^0\gamma$

Parameter	$\eta\gamma$	$\pi^0\gamma$
$\sigma_\rho^{(0)}$, nb	0.145 ± 0.063	$0.708^{+0.146}_{-0.134}$
$\sigma_\omega^{(0)}$, nb	$0.299^{+0.175}_{-0.124}$	$154.82^{+3.29}_{-3.24}$
$\sigma_\phi^{(0)}$, nb	$22.791^{+0.220}_{-0.238}$	5.30 ± 0.16
$\sigma_{\omega'}^{(0)}$, nb	–	$0.139^{+0.048}_{-0.051}$
m_ϕ , MeV	1019.52 ± 0.05	1019.46 (fixed)
m_ω , MeV	782.59 (fixed)	783.20 ± 0.13
$\varphi_{\phi-\omega}$, $^\circ$	180 (fixed)	164.4 ± 7.9
$\chi^2/\text{n.d.f.}$	72.3/82	74.0/80

respectively [12]. The energy dependence of the $\omega'(1420)$ width is calculated assuming the $\omega' \rightarrow \rho\pi$ decay. Its mass and width were fixed at the world average values of 1425 MeV and 215 MeV, respectively [12].

3.2 Results of the fits

For the fit to the $e^+e^- \rightarrow \eta\gamma$ cross section the resonance cross sections at the peak $\sigma_\rho^{(0)}$, $\sigma_\omega^{(0)}$, $\sigma_\phi^{(0)}$ as well as the ϕ meson mass m_ϕ are free parameters. The ρ and ω meson phases are chosen to be $\varphi_\rho = \varphi_\omega = 0^\circ$ while that for the ϕ meson is $\varphi_\phi = 180^\circ$ in agreement with the quark model. The values of the other parameters are taken from Ref. [12]. We also consider a model in which in addition to the parameters described above there is a contribution tentatively referred to as that of the $\rho'(1450)$ meson. A fit in the model with the $\rho'(1450)$ doesn't improve χ^2 and results in the value of $\sigma_{\rho'}^{(0)}$ consistent with zero, $\sigma_{\rho'}^{(0)} = 0.001^{+0.072}_{-0.001}$ nb and compatible with our result in the $3\pi^0$ mode [20] $\sigma_{\rho'}^{(0)} = 0.066 \pm 0.015$ nb. Therefore, for our final results for the $\eta\gamma$ decay we choose a model where $\sigma_{\rho'}^0 = 0$ nb, see Table 5.

For the $e^+e^- \rightarrow \pi^0\gamma$ case the fit parameters are: the cross sections at the resonance peak $\sigma_\rho^{(0)}$, $\sigma_\omega^{(0)}$, $\sigma_\phi^{(0)}$ and the ω meson mass m_ω . The $\rho - \omega$ phase is fixed to the value 13.3° obtained in our study of the process $e^+e^- \rightarrow \pi^+\pi^-$ [26]. The $\phi - \omega$ phase is a fit parameter. A fit, which includes a possible ω' contribution, gives the best χ^2 at the value of $\sigma_{\omega'}^{(0)}$ significantly differing from zero. Results of the best fit are shown in the last column of Table 5.

3.3 Systematic errors

There are two types of systematic uncertainties on the cross section σ_V^0 : experimental and model uncertainties. The main sources of experimental systematic errors are listed below. The systematic error due to selection criteria is 4% estimated by varying the photon energy threshold, total energy deposition, total momentum, and χ^2 . A possible uncertainty because of the method of process separation was estimated to be 3% by comparing our results obtained from fitting the distributions of the two-photon invariant mass to those from Dalitz plot analysis. The latter method also allows to determine the cross section of the QED process $e^+e^- \rightarrow 3\gamma$ and it appears to be consistent with the theoretical prediction [30]: $\sigma(3\gamma)_{\text{exp}}/\sigma(3\gamma)_{\text{th}} = 0.973 \pm 0.018$. The uncertainty in the determination of the integrated luminosity is 1% and comes from the selection criteria of Bhabha events, radiative corrections and calibrations of DC and BC. The error of the NT efficiency was estimated to be 2% by trying various fitting functions for energy dependence and variations of the cluster threshold. The 1% uncertainty of the radiative corrections comes from the dependence on the emitted photon energy and the accuracy of the theoretical formulae. In total, the experimental systematic uncertainty of the cross section is 6%.

The model uncertainty estimated by comparing the values of the cross section at the resonance peak in various models differing by the values of phases and resonance parameters was 1% (2%) for the ρ , 3%(0.1%) for the ω and 0.1%(5%) for the ϕ meson in the $\eta\gamma$ and $\pi^0\gamma$ decay modes, respectively.

4 Discussion

In Table 6 we present our results in terms of the product of the branching ratios $\mathcal{B}(V \rightarrow e^+e^-) \times \mathcal{B}(V \rightarrow P\gamma)$, where $P = \eta(\pi^0)$, which is calculated from $\sigma_V^{(0)}$ according to (3). For the $\eta\gamma$ mode one should additionally take into account the branching ratio of the $\eta \rightarrow \gamma\gamma$ decay taking its value $\mathcal{B}(\eta \rightarrow \gamma\gamma) = (39.43 \pm 0.26)\%$ from Ref. [12]. For the $\pi^0\gamma$ mode the corresponding value $\mathcal{B}(\pi^0 \rightarrow \gamma\gamma) = (98.798 \pm 0.032)\%$ from Ref. [12] was included at the MC generation stage. Our results are in good agreement with the world average values [12].

By dividing the product of the branching ratios above by the corresponding world average leptonic width from Ref. [12] one can obtain the branching ratios of the radiative decays confronted in Table 7 to the world average values [12].

Table 6

 $\mathcal{B}(V \rightarrow e^+e^-) \times \mathcal{B}(V \rightarrow P\gamma)$

Decay	This work	PDG-2004
$\rho \rightarrow \eta\gamma, 10^{-8}$	$1.50 \pm 0.65 \pm 0.09$	1.38 ± 0.17
$\omega \rightarrow \eta\gamma, 10^{-8}$	$3.17_{-1.31}^{+1.85} \pm 0.21$	3.53 ± 0.35
$\phi \rightarrow \eta\gamma, 10^{-6}$	$4.093_{-0.043}^{+0.040} \pm 0.247$	3.85 ± 0.07
$\rho \rightarrow \pi^0\gamma, 10^{-8}$	$2.90_{-0.55}^{+0.60} \pm 0.18$	2.8 ± 0.6
$\omega \rightarrow \pi^0\gamma, 10^{-6}$	$6.47 \pm 0.14 \pm 0.39$	$6.37_{-0.15}^{+0.17}$
$\phi \rightarrow \pi^0\gamma, 10^{-7}$	$3.75 \pm 0.11 \pm 0.29$	3.67 ± 0.28

Table 7

 $\mathcal{B}(V \rightarrow P\gamma)$

Decay	This work	PDG-2004
$\rho \rightarrow \eta\gamma, 10^{-4}$	$3.21 \pm 1.39 \pm 0.20$	3.0 ± 0.4
$\omega \rightarrow \eta\gamma, 10^{-4}$	$4.44_{-1.83}^{+2.59} \pm 0.28$	4.9 ± 0.5
$\phi \rightarrow \eta\gamma, 10^{-2}$	$1.373 \pm 0.014 \pm 0.085$	1.295 ± 0.025
$\rho \rightarrow \pi^0\gamma, 10^{-4}$	$6.21_{-1.18}^{+1.28} \pm 0.39$	6.0 ± 1.3
$\omega \rightarrow \pi^0\gamma, 10^{-2}$	$9.06 \pm 0.20 \pm 0.57$	$8.92_{-0.24}^{+0.28}$
$\phi \rightarrow \pi^0\gamma, 10^{-3}$	$1.258 \pm 0.037 \pm 0.077$	1.23 ± 0.10

Taking into account a variation of the m_ω and m_ϕ in various models as well as a systematic error caused by the uncertainties of the beam energy calibration, we obtain for the resonance masses:

$$m_\omega = 783.20 \pm 0.13 \pm 0.16 \text{ MeV}, \quad (4)$$

$$m_\phi = 1019.52 \pm 0.05 \pm 0.05 \text{ MeV}, \quad (5)$$

consistent with the world average values $782.59 \pm 0.11 \text{ MeV}$ and $1019.456 \pm 0.020 \text{ MeV}$, respectively [12].

Our result for the cross section of the process $e^+e^- \rightarrow \eta\gamma$ at the peak of the ϕ meson can be combined with the independent measurement of the same quantity in the decay mode $\eta \rightarrow 3\pi^0$ performed at CMD-2 [20] to obtain the ratio of the branching fractions of the η meson, $\mathcal{B}(\eta \rightarrow 3\pi^0)/\mathcal{B}(\eta \rightarrow \gamma\gamma)$. Since in both cases the η meson decays into neutral particles only, most of systematic uncertainties will cancel in such a ratio:

$$\frac{\mathcal{B}(\eta \rightarrow 3\pi^0)}{\mathcal{B}(\eta \rightarrow \gamma\gamma)} = 0.817 \pm 0.012 \pm 0.032, \quad (6)$$

which is consistent with the world average value 0.825 ± 0.007 [12].

5 Conclusions

- Using a data sample corresponding to integrated luminosity of 21 pb^{-1} , the cross sections of the processes $e^+e^- \rightarrow \eta\gamma, \pi^0\gamma$ have been measured in the c.m. energy range 600–1380 MeV. The following branching ratios have been determined:

$$\begin{aligned}\mathcal{B}(\rho^0 \rightarrow \eta\gamma) &= (3.21 \pm 1.39 \pm 0.20) \cdot 10^{-4}, \\ \mathcal{B}(\omega \rightarrow \eta\gamma) &= (4.44_{-1.83}^{+2.59} \pm 0.28) \cdot 10^{-4}, \\ \mathcal{B}(\phi \rightarrow \eta\gamma) &= (1.373 \pm 0.014 \pm 0.085) \cdot 10^{-2}, \\ \mathcal{B}(\rho^0 \rightarrow \pi^0\gamma) &= (6.21_{-1.18}^{+1.28} \pm 0.39) \cdot 10^{-4}, \\ \mathcal{B}(\omega \rightarrow \pi^0\gamma) &= (9.06 \pm 0.20 \pm 0.57) \cdot 10^{-2}, \\ \mathcal{B}(\phi \rightarrow \pi^0\gamma) &= (1.258 \pm 0.037 \pm 0.077) \cdot 10^{-4}.\end{aligned}$$

- The values of the ω and ϕ meson masses are:

$$\begin{aligned}m_\omega &= 783.20 \pm 0.13 \pm 0.16 \text{ MeV}, \\ m_\phi &= 1019.52 \pm 0.05 \pm 0.05 \text{ MeV}.\end{aligned}$$

- From the two independent measurements of the $\phi \rightarrow \eta\gamma$ decay the following ratio of the branching ratios of the η meson has been obtained:

$$\mathcal{B}(\eta \rightarrow 3\pi^0)/\mathcal{B}(\eta \rightarrow \gamma\gamma) = 0.817 \pm 0.012 \pm 0.032.$$

Acknowledgements

The authors are grateful to the staff of VEPP-2M for the excellent performance of the collider, and to all engineers and technicians who participated in the design, commissioning and operation of CMD-2. This work is supported in part by grants DOE DEFG0291ER40646, NSF PHY-0100468, PST.CLG.980342, RFBR-03-02-16280, RFBR-03-02-16477, RFBR-03-02-16843, RFBR-04-02-16217, and RFBR-04-02-16223-a.

References

- [1] T. Ohshima, Phys. Rev. D 22 (1980) 707.
- [2] P.J. O'Donnell, Rev. Mod. Phys. 53 (1981) 673.
- [3] A. Bramon, A. Grau, G. Pancheri, Phys. Lett. B 344 (1995) 240.

- [4] M. Hashimoto, Phys. Rev. D 54 (1996) 5611.
- [5] M. Benayoun, S.I. Eidelman, V.N. Ivanchenko, Z. Phys. C 72 (1996) 221.
- [6] P. Ball, J.M. Frere, M. Tytgat, Phys. Lett. B 365 (1996) 367.
- [7] A. Bramon, R. Escribano, M.D. Scadron, Eur. Phys. J. C 7 (1999) 271.
- [8] M. Benayoun, Phys. Rev. D 59 (1999) 114027.
- [9] M. Davier, et al., Eur. Phys. J. C 31 (2003) 503.
- [10] T. Barnes, et al., Phys. Rev. D 55 (1997) 4157.
- [11] F. Close, A. Donnachie, Yu.S. Kalashnikova, Phys. Rev. D 67 (2003) 074031.
- [12] S. Eidelman et al., Phys. Lett. B 592 (2004) 1.
- [13] V.P. Druzhinin, et al., Phys. Lett. 144 B (1984) 136.
- [14] S.I. Dolinsky et al., Z. Phys. C42 (1989) 511.
- [15] M.N. Achasov et al., Eur. Phys. J. C 12 (2000) 25.
- [16] M.N. Achasov et al., Phys. Lett. B 559 (2003) 171.
- [17] G. A. Aksenov et al., Preprint Budker INP 85-118, Novosibirsk, 1985;
E. V. Anashkin et al., ICFA Instr. Bulletin 5 (1988) 18.
- [18] R. R. Akhmetshin et al., Preprint Budker INP 99-11, Novosibirsk, 1999.
- [19] E.V. Anashkin et al., Preprint Budker INP 99-1, Novosibirsk, 1999.
- [20] R.R. Akhmetshin et al., Phys. Lett. B 509 (2001) 217.
- [21] R.R. Akhmetshin et al., Phys. Lett. B 508 (2001) 217.
- [22] R.R. Akhmetshin et al., Phys. Lett. B 551 (2003) 27.
- [23] R.R. Akhmetshin et al., Phys. Lett. B 562 (2003) 173.
- [24] R.R. Akhmetshin et al., Phys. Lett. B 580 (2004) 119.
- [25] E. A. Kuraev and V.S. Fadin, Sov. J. Nucl. Phys., 41 (1985) 466.
- [26] R.R. Akhmetshin et al., Phys. Lett. B 578 (2004) 285.
- [27] G. J. Gounaris and J.J. Sakurai, Phys. Rev. Lett. 21 (1968) 244.
- [28] R.R. Akhmetshin et al., Phys. Lett. B 434 (1998) 426.
- [29] R.R. Akhmetshin et al., Phys. Lett. B 466 (1999) 392.
- [30] S.I. Eidelman and E.A. Kuraev, Nucl. Phys. B 143 (1978) 353.